
## Dyed Green BERYL

Emerald simulants and synthetic emeralds have often been submitted for testing to GIA (e.g., Spring 2001 Lab Notes, pp. 57–59). Recently, the New York laboratory examined a dyed green beryl that was intended to imitate natural emerald. The green octagonal step-cut stone, set in a yellow metal ring with near-colorless stones, initially appeared to be emerald.

The stone had a refractive index of 1.588–1.595 and fluoresced a very weak chalky yellow under long-wave UV radiation and a weak chalky yellow under short-wave UV. Microscopic examination revealed the obvious presence of a green dye concentration in numerous fractures (figure 1) and other natural beryl inclusions such as short needles, particles, and jagged fingerprint patterns. This dyed green material also enhanced the clarity of the stone.

In addition, dyed bands (~610 and 660 nm) were revealed in the visible spectrum by utilizing a high-resolution visible spectrometer (figure 2). The green color in this sample was caused by an organic dye rather than chromium or vanadium elements that give rise to a green color in natural emeralds. When the color was observed under a diffused light source, it became apparent that a near-colorless natural beryl was the starting material. This example shows the importance of spectroscopic testing to confirm the cause of an emerald's color.

*HyeJin Jang-Green*

*Figure 1. A green dye concentration in beryl was observed along fractures and confirmed by spectroscopic testing.*

## DIAMONDS

### Coesite Inclusions with Filaments in Diamond

GIA's New York lab recently encountered an HPHT-treated Fancy Vivid yellow diamond with unique inclusions. The diamond was determined to be HPHT-treated due to the presence of a strong solitary peak at 1344 $cm^{-1}$ in the infrared absorption spectrum, indicating isolated nitrogen C-

*Figure 2. In the beryl's Vis-NIR absorption spectrum, dye bands were observed at ~610 and 660 nm, while sharp Cr-related features were absent.*

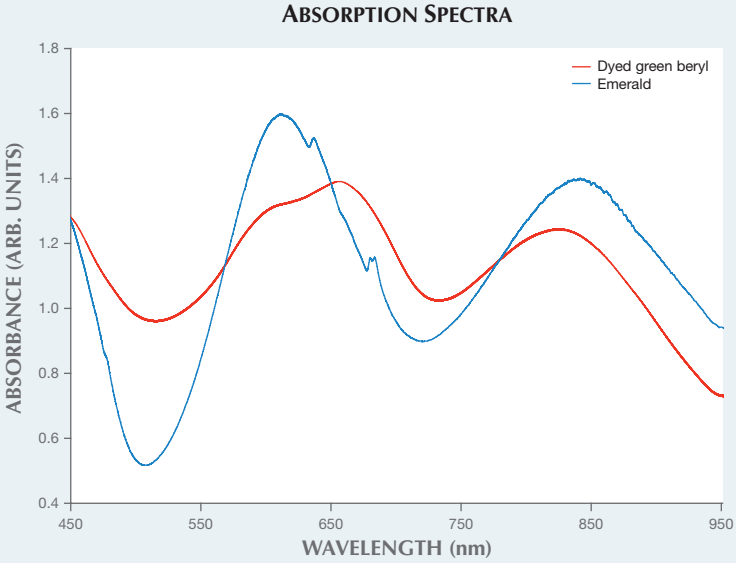


*Editors' note: All items were written by staff members of GIA laboratories.*

GEMS & GEMOLOGY, Vol. 52, No. 4, pp. 410–421.

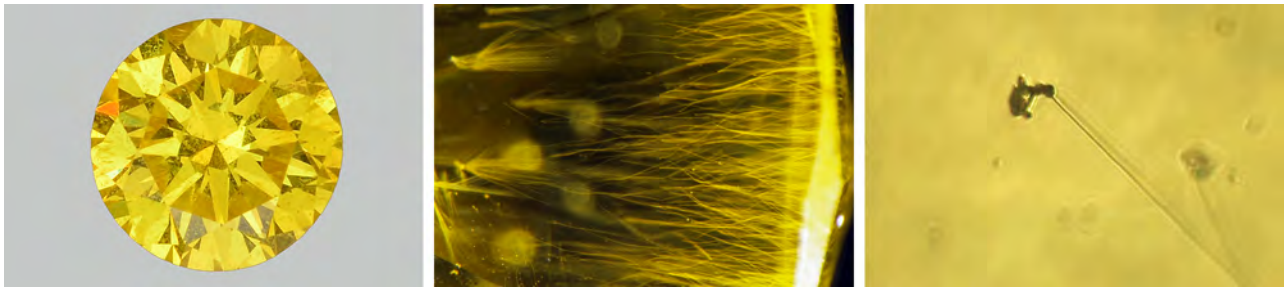

*Figure 3. Left: A Vivid yellow 0.164 ct diamond containing coesite inclusions. The diamond is 3.52 mm in diameter. Center: Photomicrograph of a dense region of coesite inclusions with filaments; field of view 1.26 mm. Right: A photomicrograph of a single coesite inclusion, with filament gradually going out of focus to the right; field of view 100 µm.*

centers, a relatively even distribution of color, and the absence of certain peaks in the diamond's Raman spectrum. However, the color treatment of this diamond was not its most interesting aspect. The diamond was unique for possessing many small inclusions with fine, tail-like filaments (figure 3). Visually, the filaments within this 0.164 ct round brilliant-cut diamond resembled horsetail inclusions in demantoid garnet. Raman spectroscopy of four separate inclusions gave peaks for coesite, a high-pressure $SiO_2$ polymorph (figure 4).

The measured peaks of coesite are shifted with respect to reference spectra due to high confining pressures within each inclusion. The shift of the main peak from its unconstrained position at 521 $cm^{-1}$ to the measured peak in the inclusions, at 533 ± 1 $cm^{-1}$, can be used to calculate the internal pressure, which is an incredible 4.3 ± 0.4 GPa (R.J. Hemley, "Pressure dependence of Raman spectra of $SiO_2$ polymorphs: α-quartz, coesite, and stishovite," in M.H. Manghnani and Y. Syono, Eds., *High-Pressure Research in Mineral Physics*, AGU, Washington, D.C., pp. 347–359). When a diamond is carried to the surface, the diamond and its inclusions do not decompress coherently, so it is fairly common for inclusions to have some amount of "locked-in" remnant pressure. HPHT treatment is unlikely to have modified this remnant pressure, although the possibility cannot be entirely ruled out without more detailed study. These particular coesite inclusions preserve an especially high pressure because the inclusions are small. Larger inclusions are more likely to crack or deform the surrounding diamond and relieve some of the built-up pressure.

Coesite inclusions are not uncommon in diamond, and they are interpreted to indicate an eclogitic mantle host rock paragenesis. The curvilinear filaments extending from the inclusions are, however, both uncommon and unusual. They have a preferred orientation, extending to the right in figure 3 (center). This direction corresponds with the interpreted direction of growth, outward from the center of the diamond. Most filaments are singular, measuring 20–200 µm long, but a few branch into a fan-like spray of sub-parallel filaments. The thickness of each filament is less than 1 µm, making it difficult to observe or characterize them in more detail. Interestingly, the inclusions occur within discrete regions in the diamond, which correspond to cuboid {100} growth sectors when examined in the DiamondView (short-wave UV fluo-

*Figure 4. Raman spectra of four inclusions corresponding to coesite with high remnant pressure inside each inclusion. Spectra have been vertically offset for clarity.*

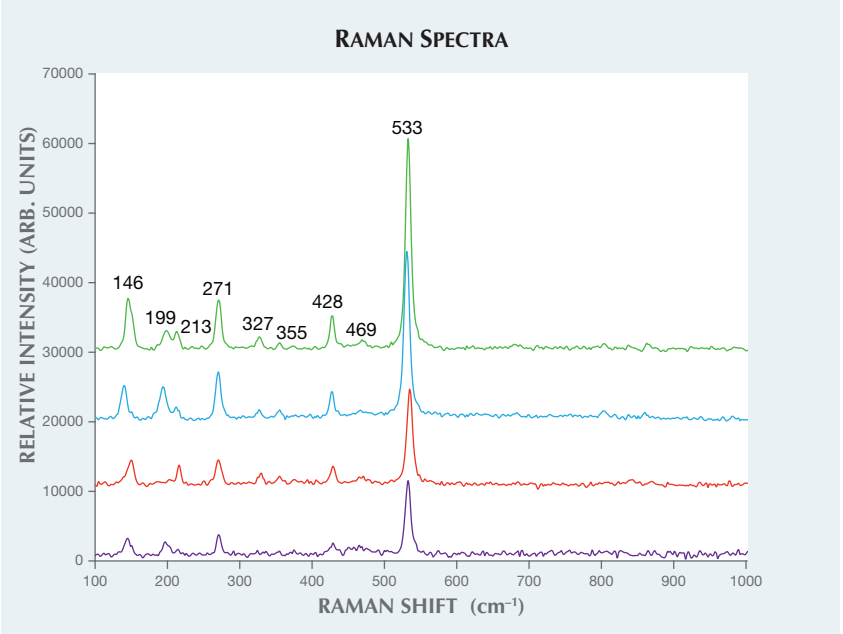

rescence imaging). A possible explanation for the filaments is that they are grown-in dislocations, originating from the point where the diamond just finished enveloping each inclusion. The filaments resemble the dislocations seen in X-ray topography of natural diamonds (e.g., B. Rondeau et al., "On the growth of natural octahedral diamond upon a fibrous core," *Journal of Crystal Growth*, Vol. 304, 2007, pp. 287–293). A dislocation alone, however, would not be optically visible. Small amounts of solid or fluid material trapped with the dislocation might be responsible for its visibility.

*Evan M. Smith, Christopher Vendrell, and Paul Johnson*

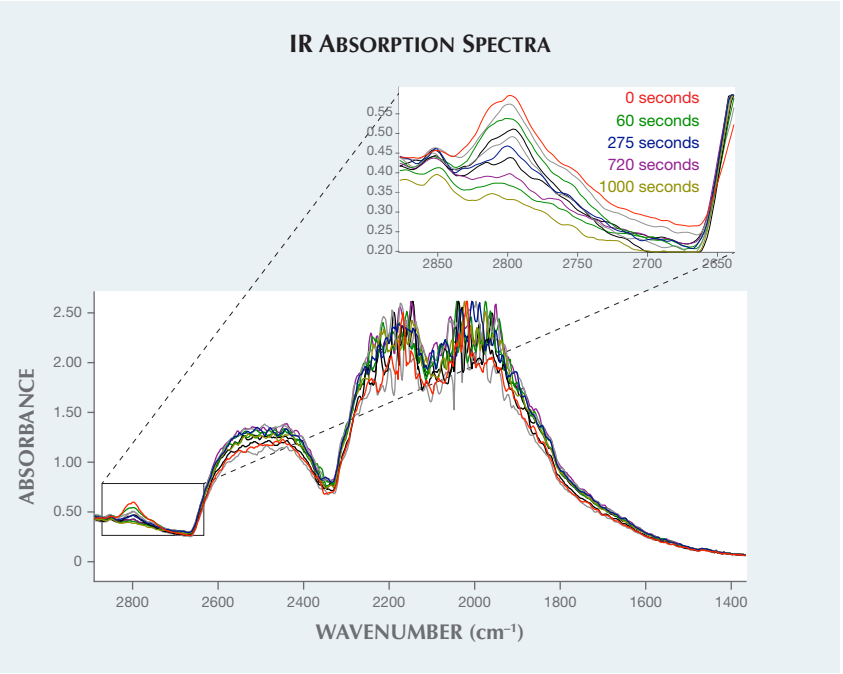


*Figure 5. In response to UV excitation, the IR absorption spectra for a 1.01 ct Fancy gray, nominally type IIa diamond shows a pronounced peak at 2800 cm$^{-1}$, associated with type IIb diamond and boron impurities. The intensity of the 2800 cm$^{-1}$ peak decays over several minutes. For the sake of clarity, not all collected IR absorption spectra are shown here; the peak at 2850 cm$^{-1}$ is unrelated to boron and is caused by hydrocarbon contamination on the diamond surface.*

## Decay Kinetics of Boron-Related Peak in IR Absorption of Natural Diamond

Recently, gemologists at the National Gold & Diamond Testing Center in China found that the uncompensated boron peak at 2800 cm$^{-1}$ in FTIR absorption could be induced by UV excitation and then subsequent decay, similar to the phosphorescence response often seen in type IIb diamonds (J. Li et al., "A diamond with a transient 2804 cm$^{-1}$ absorption peak," *Journal of Gemmology*, Vol. 35, 2016, pp. 248–252).

The Carlsbad laboratory recently received a nominally type IIa, 1.01 ct diamond with Fancy gray color. It was identified as natural and, uncharacteristically, showed a 500 nm band phosphorescence, which is typical for type IIb diamonds (S. Eaton-Magaña and R. Lu, "Phosphorescence of type IIb diamonds," *Diamond and Related Materials*, Vol. 20, 2011, pp. 983–989). With UV excitation we recorded the transient 2800 cm$^{-1}$ absorption (associated with uncompensated boron) observed in type IIb diamonds, and we monitored the peak's decay (figure 5).

From the calculated area of the 2800 cm$^{-1}$ absorption peak, we can determine the uncompensated boron (Bo) concentration (D. Fisher et al., "Brown colour in natural diamond and interaction between the brown related and other colour-inducing defects," *Journal of Physics: Condensed Matter*, Vol. 21, 2009, 364213). Immediately after UV excitation, the diamond showed blue phosphorescence and the FTIR spectrum changed from a nominally type IIa diamond to a type IIb, with an uncompensated boron concentration of ~70 ppb (figure 6, left). An increase in the 2800 cm$^{-1}$ peak upon UV excitation was previously recorded in some other type IIb diamonds as well and in a few other nominally type IIa diamonds examined by GIA, but those showed much lower values than this sample with UV excitation, with an initial increase in Bo of ~5 ppb or less. The decay of the 2800 cm$^{-1}$ absorption band in the diamond studied here was well described by the non-exponential decay model $1/(1+kt)$, where $t$ is the decay time and $k$ is a constant. This equation fit the absorption decay data better than an exponential decay model or the hyperbolic decay model that describes type IIb diamond phosphorescence, $1/(1+kt)^2$ (K. Watanabe et al., "Phosphorescence in high-pressure synthetic diamond," *Diamond and Related Materials*, Vol. 6, 1997, pp. 99–106).

Photoluminescence spectra were collected both with and without UV exposure using 488, 514, and 830 nm excitation. The only distinction observed between the two sets of spectra was the addition of a 3H peak (503.5 nm) when the diamond was exposed to UV radiation. The 3H peak is ascribed as an intrinsic defect containing interstitials and is often observed in PL spectra of type IIb diamonds.

Phosphorescence spectra were also recorded (figure 6, right). As expected based on prior research of diamond phosphorescence, the data did correspond well with the hyperbolic model. When boron impurities are present but are electrically compensated by other defects such as nitro-

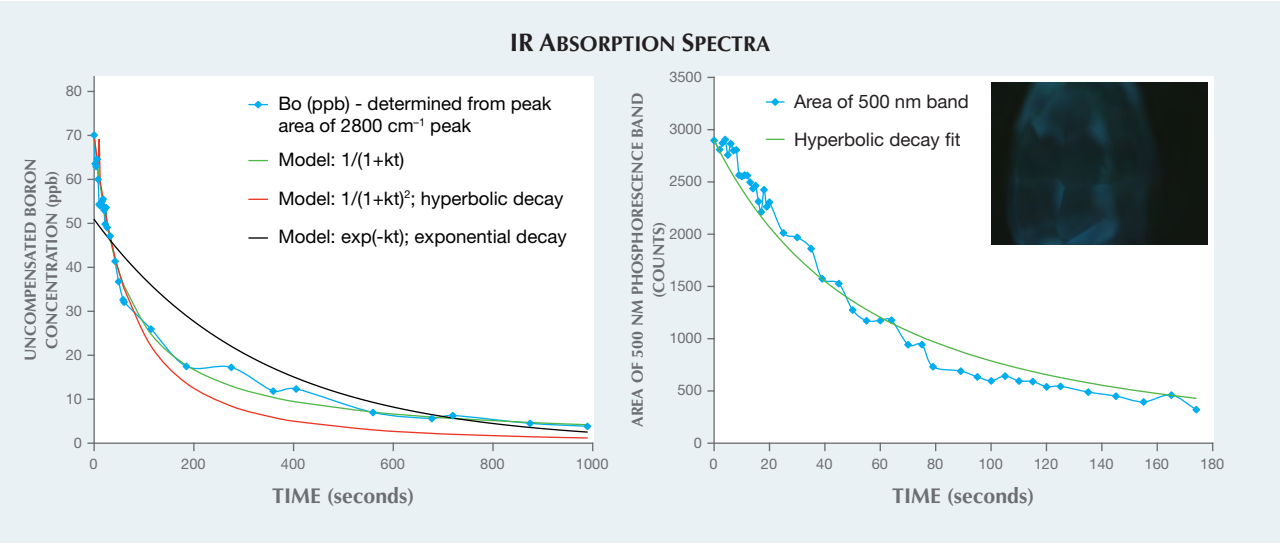


*Figure 6. Left: The uncompensated boron concentration for the IR absorption spectra in figure 5 were calculated and compared against several phosphorescence decay models. Right: The decay of the phosphorescence peak at 500 nm, also induced by UV excitation, was calculated and compared against the accepted model for phosphorescence. The DiamondView image shows the diamond's blue phosphorescence.*

gen, the 2800 $cm^{-1}$ peak would not be detected and a nominally type IIa diamond would be recorded by IR absorption. However, UV excitation creates a charge transfer effect, temporarily uncompensating some of the boron so that the Bo concentration temporarily increases. This absorption decay of the 2800 $cm^{-1}$ peak is most dramatic in nominally type IIa diamonds such as this sample, but has also been observed to a lesser extent in type IIb diamonds. There are several unanswered questions regarding the phosphorescence mechanism and decay kinetics in type IIb diamonds, and further study of this absorption decay will help address these issues.

*Sally Eaton-Magaña*

## Update on Spectroscopy of "Gold Sheen" SAPPHIRES

Sapphires displaying a golden sheen, known in the trade as "gold sheen" or "Zawadi" sapphires, entered the gem market in late 2009. These sapphires are mined in eastern Kenya (T.N. Bui et al., "From exsolution to 'gold sheen': A new variety of corundum," *Journal of Gemmology*, Vol. 34, No. 8, 2015, pp. 678–691). They contain dense needles and platelets of hematite/ilmenite inclusions, which are responsible for producing a golden shimmer on the surface.

Recently, GIA's laboratory in Bangkok received 14 gold sheen sapphires of various shapes and cuts. The samples had yellow and green to blue bodycolor, were transparent to translucent, and weighed 1.06 to 97.69 ct (figure 7). Their physical properties and inclusions were similar to those of gold

*Figure 7. These 14 sapphires, weighing up to 97.69 ct each, displayed a golden sheen effect and in some cases six-rayed asterism. They possessed sufficiently large inclusion-free areas to enable good-quality spectra.*

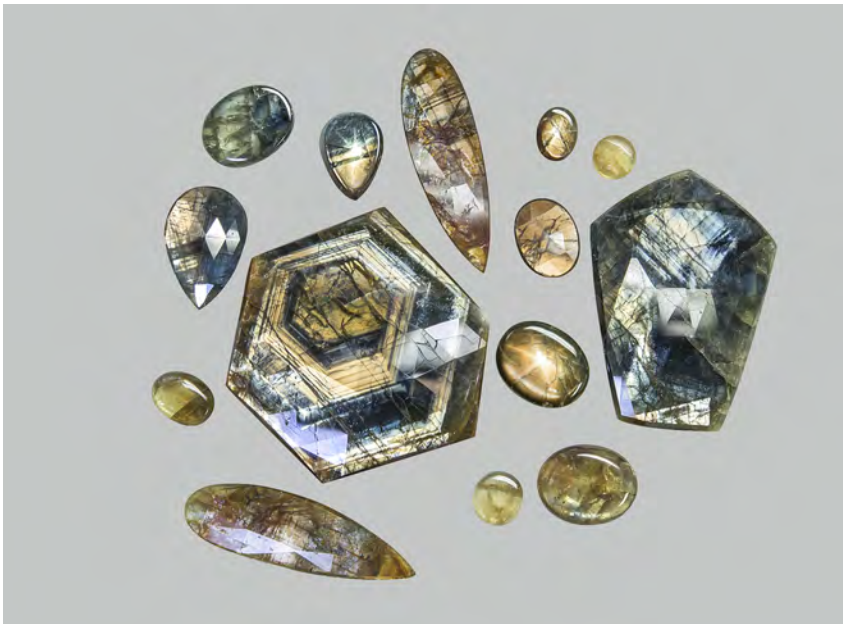

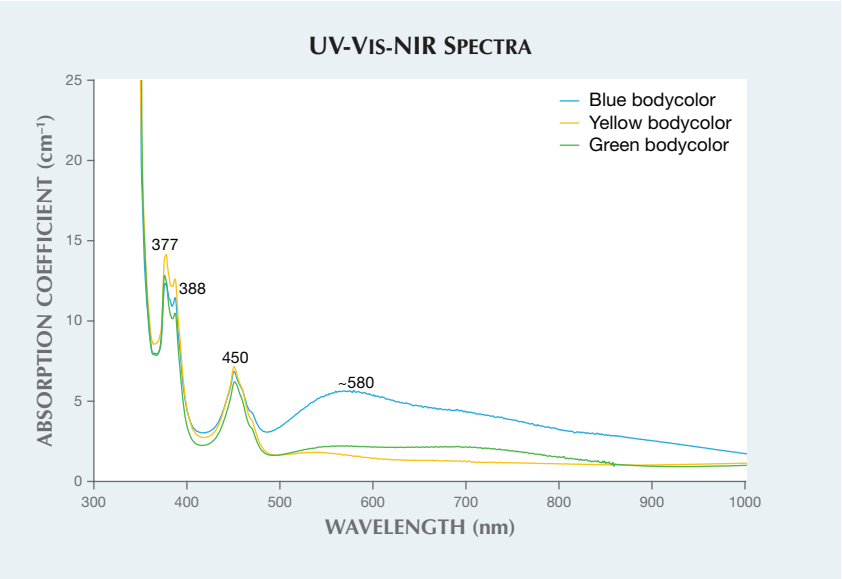


*Figure 8. The UV-Vis-NIR spectrum of a gold sheen sapphire with yellow bodycolor revealed strong Fe-related absorption features at 377, 388, and 450 nm. The spectra of green to blue samples revealed an additional $Fe^{2+}$-$Ti^{4+}$ intervalence charge-transfer band centered at around 580 nm. These samples were not specifically aligned to the c-axis.*

sheen sapphires described in Bui et al. (2015): an RI of 1.762–1.772, a birefringence of 0.008–0.009, a hydrostatic SG of 3.98–4.01, an inert reaction to long- and short-wave UV radiation, and an abundance of hematite/ilmenite platelets. Since the samples had some transparent windows, UV-Vis-NIR spectra were analyzed.

The UV-Vis-NIR spectra all displayed strong Fe-related absorption features at 377, 388, and 450 nm. Samples with a yellow bodycolor showed mainly the three Fe features, whereas the green to blue sapphires revealed a band centered at around 580 nm that is related to $Fe^{2+}$-$Ti^{4+}$ intervalence charge transfer, in addition to the three strong Fe features (figure 8). LA-ICP-MS analysis on inclusion-free areas showed high Fe ranging from 2550 to 3260 ppma, 2 to 8 ppma Mg, 4 to 11 ppma Ti, 30 to 45 ppma Ga, and 0.2 to 0.7 ppma V. For the green to blue samples, Ga/Mg overlapped, varying from 5 to 30. Samples with a yellow bodycolor varied from 4 to 11. Other trace elements including Zr, Nb, Ta, W, Th, and U were also detected but in insignificant quantities. It is notable that Mg and Ti concentrations were comparable in the yellow samples (all $Ti^{4+}$ charges compensate $Mg^{2+}$, leaving no $Ti^{4+}$ to interact with $Fe^{2+}$), whereas Ti concentrations were significantly higher than Mg concentrations in the green to blue sapphires resulting in some $Ti^{4+}$ forming $Fe^{2+}$-$Ti^{4+}$ pairs (J.L. Emmett et al., "Beryllium diffusion of ruby and sapphire," Summer 2003 *G&G*, pp. 84–135). The chemical and UV-Vis-NIR spectroscopic features corresponded with the bodycolors of these sapphires. In addition, FTIR spectra of the gold sheen sapphires generally showed diagnostic features of AlO(OH), consistent with either boehmite or diaspore; kaolinite; and gibbsite.

*Wasura Soonthorntantikul, Ungkhana Atikarnsakul, and Vararut Weeramonkhonlert*

## SYNTHETIC DIAMONDS

### CVD Synthetic Diamond Over 5 Carats Identified

Chemical vapor deposition (CVD) technology has accelerated over the last several years, and the rapidly improving techniques have produced large, high-quality near-colorless and colorless synthetic diamonds. Two samples over 3 carats were reported in early 2016 as the largest CVD synthetics (Winter 2015 Lab Notes, pp. 437–439). GIA recently tested a CVD-grown synthetic diamond that weighed over 5 carats, marking a significant milestone.

The 5.19 ct cushion modified brilliant measuring 10.04 × 9.44 × 6.18 mm (figure 9) was submitted to GIA's Hong Kong laboratory for grading service. The stone was not disclosed as a synthetic diamond. Using the lab's standard screening and testing processes, it was identified as CVD synthetic. Following examination, a GIA Identification Report was issued and the stone was inscribed on the girdle with the report number and the words "Laboratory Grown," following GIA's protocols for undisclosed synthetics.

This is the largest CVD synthetic diamond GIA has examined to date, and the largest reported in the jewelry industry. It had J-equivalent color

*Figure 9. This 5.19 ct CVD-grown diamond (10.04 × 9.44 × 6.18 mm, with J-equivalent color and $VS_2$-equivalent clarity) is the largest CVD synthetic GIA has identified to date.*

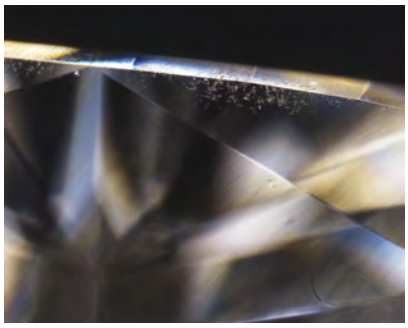

*Figure 10. Needles and pinpoints were the major internal features. Black inclusions, a common feature of CVD synthetic diamond, were not observed.*

*Figure 11. Microscopic examination between crossed polarizers revealed high-order interference colors, attributed to strong lattice dislocation.*

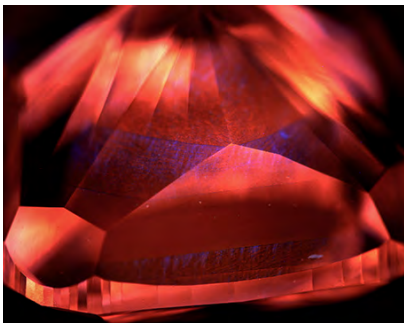

*Figure 12. Fluorescence imaging from the DiamondView showed strong red fluorescence with bundles of violet-blue. Up to six growth layers basically parallel to the table were revealed.*

grade and $VS_2$-equivalent clarity, comparable to a high-quality natural counterpart. Natural-looking internal inclusions such as needles and clouds were the major features (figure 10). Strong graining and a fracture in the table were also clearly observed under the microscope. It is worth noting that black inclusions, often contained in synthetic diamond, were not found in this CVD specimen, which could have been mistakenly identified as natural based on microscopic examination alone. This case therefore highlights the importance of using advanced spectroscopic instruments as well as conventional gemological techniques to ensure an accurate identification.

Viewing the sample under a binocular microscope with cross-polarized light revealed irregular birefringence patterns with high-order interference colors, a common feature of CVD synthetic diamond (figure 11). Fluorescence images under the short-wave UV radiation of the DiamondView showed strong red fluorescence with irregularly distributed areas of violet-blue (figure 12). The images also revealed a layered growth structure, indicating a start-stop cycling growth process typical of CVD synthesis. Up to six growth layers basically parallel to the table were identified from the fluorescence features. These multiple growth segments make it possible to grow such a thick sample.

Infrared absorption spectroscopy identified the sample as type IIa. Except for a very weak absorption at 1332 $cm^{-1}$, no other absorption features (such as hydrogen-related defects) were detected. Photoluminescence (PL) spectra were collected at liquid nitrogen temperature with various excitation wavelengths. The $SiV^-$ doublet at 736.6 and 736.9 nm, a common feature of both CVD and HPHT synthetics and only rarely seen in natural diamond, was observed using 457, 514, and 633 nm laser excitation, suggesting the sample's synthetic origin. Spectra acquired with 514 nm laser excitation also showed emissions from NV centers at 575.0 nm ($NV^0$) and 637.0 nm ($NV^-$), with the $NV^0$ center dominating in intensity (figure 13). The occurrence of a weak emission pair at 596.5 and 597.2 nm, in

*Figure 13. The photoluminescence spectrum acquired with 514 nm laser excitation revealed strong emissions from NV centers in addition to emissions from $SiV^-$. Emissions at 596/597 nm indicated that this synthetic diamond was not annealed after growth.*

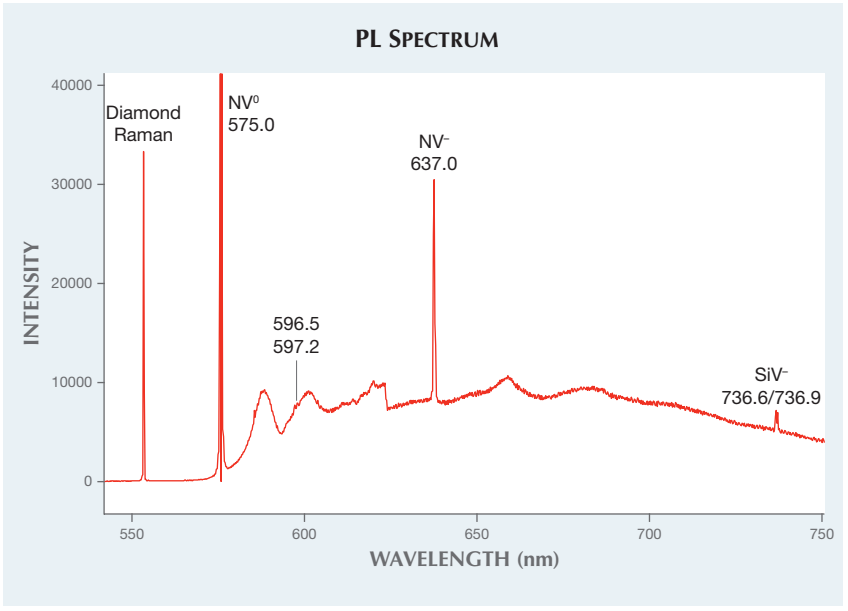

combination with the absence of H3 emission, unequivocally identified this as an as-grown CVD synthetic diamond. No post-growth annealing had been applied to improve its color appearance.

CVD synthetics are available from several sources. The gemological and spectroscopic features of this 5.19 ct sample are very similar to those GIA has examined from Washington Diamonds (now known as WD Lab Grown Diamonds). As diamond growth techniques continue to advance, we expect to see more high-quality samples, both in size and clarity.

*Billie "Pui Lai" Law and Wuyi Wang*

## Blue HPHT Synthetic Diamond Over 10 Carats

In September 2016, GIA's Hong Kong laboratory tested a 10.08 ct blue synthetic diamond grown by the high-pressure, high-temperature (HPHT) method. This was the largest HPHT synthetic diamond recorded to date. It was also the largest HPHT blue synthetic diamond GIA has examined, surpassing two samples examined by the Hong Kong lab in May 2016 (Summer 2016 Lab Notes, pp. 195–196). The manufacturer of all three stones is New Diamond Technology (NDT) in St. Petersburg, Russia.

The 10.08 ct emerald cut measured 13.54 × 11.39 × 7.36 mm and had a color grade equivalent to Fancy Deep blue (figure 14). The client submitted the stone for scientific examination and disclosed that it was a synthetic diamond. Magnification revealed very weak color zoning with a banded structure. A few very small metallic inclusions and fractures were observed, resulting in a clarity grade equivalent to $SI_1$. Microscopic examination with crossed polarizers showed no detectable strain, indicating a very low density of dislocations. Fluorescence images collected using the DiamondView revealed the distinctive "hourglass" growth pattern, which is significant in revealing HPHT growth. Strong blue phosphorescence, another indicator, was also detected. These images were dominated by the {111} growth sector, which had much stronger blue fluorescence. The {100} growth sector with very weak fluorescence was much smaller, indicating this synthetic diamond was produced with octahedral growth. It also exhibited a strong red-orange fluorescence to long-wave UV radiation and a yellow fluorescence to short-wave UV (figure 15), both of which are uncommon.

Infrared absorption spectroscopy confirmed this was a type IIb diamond, with a strong absorption band at ~2800 $cm^{-1}$ in its infrared absorption spectrum attributed to boron impurity. PL analysis conducted at liquid nitrogen temperature with varying laser excitations showed it was surprisingly pure, with no detectable impurity-related emissions.

Based on these gemological and spectroscopic features, we concluded that this sample was an HPHT synthetic diamond. This offered another indication of the rapid progress in HPHT synthetic technology, which offers an option for the diamond jewelry industry as well as many promising industrial and research applications. NDT also plans to offer large colorless and blue HPHT-grown diamonds made from unique donor carbon "DNA," such as car leather and wood trim that have been turned into ultra-clean graphite. With standard protocols in place at GIA laboratories, every type of synthetic diamond on the market can be confidently identified.

*Figure 14. This 10.08 ct (13.54 × 11.39 × 7.36 mm) HPHT-grown diamond, with color equivalent to Fancy Deep blue, is the largest HPHT synthetic to date.*

*Terry "Ping Yu" Poon and Wuyi Wang*

## Mixing of Natural Diamonds with HPHT Synthetic Melee

In recent years, significant amounts of colorless to near-colorless HPHT-grown synthetic diamond melee have been produced for the jewelry indus-

*Figure 15. The blue synthetic diamond showed strong red-orange fluorescence to long-wave UV radiation (left) and yellow fluorescence to short-wave UV.*

*Figure 16. These 23 HPHT-grown synthetic diamond melee, ranging from 0.002 to 0.012 ct, were identified recently at GIA's Hong Kong lab.*

try. As a result, the separation of natural from synthetic melee diamonds has become increasingly critical. GIA offers melee diamond screening services using conventional gemological techniques and analytical methods such as photoluminescence and infrared absorption spectroscopy. In September 2016, GIA's Hong Kong laboratory received 135 melee diamonds for identification service (see figure 16). Of these, 131 were confirmed to be HPHT synthetics and four were natural diamonds. It is interesting to find natural diamonds mixed in HPHT-dominated groups as "contamination."

The tested melee were colorless to near-colorless round brilliants, ranging from 0.002 to 0.012 ct. Infrared absorption spectroscopy performed on the 131 HPHT synthetics showed they were generally type IIb with a very weak absorption band at ~2800 $cm^{-1}$ from trace boron in the diamond lattice. Blue phosphorescence with varying intensity was observed under short-wave UV radiation (<225 nm) and could be easily detected in the DiamondView (figure 17). In photoluminescence spectroscopy collected at liquid nitrogen temperature, clear emissions from $SiV^-$ at 736.6/736.9 nm were recorded using 633 nm laser excitation, and extremely strong Ni-related emissions at 882/884 nm occurred in all 131 synthetic melee. These features are similar to those observed from known HPHT synthetic diamonds from a few sources in China.

The four natural diamonds showed no phosphorescence under short-wave UV radiation. When examined in the DiamondView, they displayed blue fluorescence and very weak phosphorescence. Infrared absorption spectroscopy indicated these stones were type IIa, and no trace boron absorption was recorded. In photoluminescence analysis, no $SiV^-$ emission was detected. Surprisingly, all four diamonds showed weak Ni-related emissions at 882/884 nm. Their most notable photoluminescence feature was an extremely broad band centered at ~700 nm, which is usually observed in natural diamonds.

*Figure 17. Phosphorescence in an HPHT-grown synthetic diamond melee.*

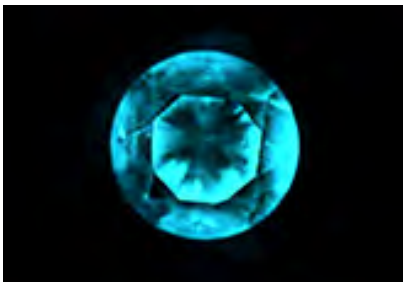

*Figure 18. This DiamondView image of the 1.60 ct HPHT synthetic shows the diagnostic square pattern seen in the crown facets.*

We would expect to find a small percentage of HPHT synthetics mixed in with natural diamond melee, but on a few occasions we have seen the opposite. As GIA launches the melee sorting service, we anticipate that more melee goods will be submitted for natural vs. synthetic diamond testing.

*Terry Poon, Carmen Lo, and Billie Law*

### HPHT-Grown Synthetic with Strain

An undisclosed HPHT-grown synthetic diamond was submitted to the GIA laboratory in Ramat Gan, Israel, for a diamond grading report. It weighed 1.60 ct and was in the near-colorless range. Initial screening showed the diamond was type IIa (without detectable nitrogen or boron in the infrared spectrum), which prompted further testing. Examination with the DiamondView fluorescent imaging system revealed the growth patterns betraying the synthetic origin (figure 18). Photoluminescence detected a further lack of impurities: no nickel-related peaks, a very common defect in HPHT synthetics, and only small amounts of nitrogen-vacancy centers.

*Figure 19. An image taken with polarized light showing the linear birefringence colors, indicating the presence of linear strain in the diamond lattice. Field of view 6 mm.*

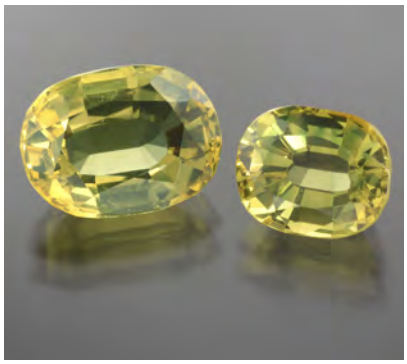

*Figure 20. These two doublets, a 6.45 ct greenish yellow oval mixed cut and a 4.17 ct greenish yellow cushion mixed cut, contained a synthetic spinel crown and a synthetic sapphire pavilion.*

When viewed under polarized light, the diamond showed very little strain throughout most of the body, but one side on the pavilion displayed noticeable birefringent colors caused by internal strain (figure 19). HPHT-grown synthetic diamonds are known for being mostly free of strain, which generally occurs only around inclusions. They are grown in a metal catalyst, and metal particles can become trapped in them. These trapped particles place stress on the host diamond, which causes strain. But that is a localized strain seen around an inclusion, which was not the case in this synthetic diamond. Except for a small fracture on the pavilion, there were no internal inclusions that could have created strain. Furthermore, the strain patterns were linear rather than radial, as is the case with inclusion-related strain.

Fortunately, this strain is still distinguishable from the type of strain in natural diamonds, which have a cross-hatched pattern known as "tatami" strain. The cause of the strain in this synthetic diamond is unknown, but if it is related to a new growth process we would expect to see more strained HPHT-grown diamonds in the future. As innovations in the synthetic diamond industry continue to introduce a wider variety of products, more and more properties of natural and synthetic diamonds will start to overlap, necessitating caution when separating stones.

*Troy Ardon and Ronny Batin*

## SYNTHETIC SAPPHIRE and SYNTHETIC SPINEL Doublets

Assemblages have been used to imitate various gemstones for many years. Some of the most common are garnet and glass doublets, sapphire and synthetic corundum doublets, synthetic spinel triplets, and beryl triplets.

The Carlsbad laboratory recently examined two uncommon doublets: a 6.45 ct greenish yellow oval mixed cut and a 4.17 ct greenish yellow cushion mixed cut (figure 20). Initial microscopic observation revealed a separation plane near both girdles with flattened, trapped gas bubbles in colorless cement (figure 21, center). The green crowns were joined to the yellow pavilions with this colorless

*Figure 21. Left: The green crown and yellow pavilions of the 6.45 ct oval mixed cut are easily observed in immersion. Center: A separation plane near the girdle with a flattened, trapped gas bubble; field of view 1.76 mm. Right: Parallel twining planes in the pavilion; field of view 2.90 mm.*

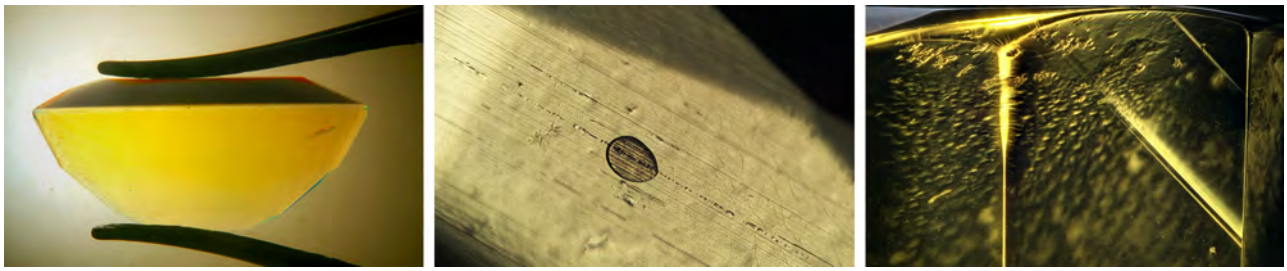

*Figure 22. This tortoiseshell scepter is from the Palais Royal collection.*

cement (figure 21, left). An RI of 1.728 and whitish chalky fluorescence under short-wave UV on both crowns were suggestive of synthetic spinel. One of the doublets showed thick green curved color banding. Photoluminescence (PL) emission spectra identified the crowns as synthetic spinel.

In both doublets, the pavilion had a refractive index of 1.760 to 1.768 and was inert to UV radiation. The two assemblages were clean and showed only twining planes (figure 21, right). Faint yellow curved color banding was visible when they were immersed in methylene iodide and observed with a blue color filter. EDXRF analysis showed a chemical composition consistent with synthetic corundum. They contained Ni as a trace element and no Fe, Ga, or Ti.

Microscopic observation and advanced gemological testing confirmed that these were doublets consisting of a synthetic spinel crown and a synthetic sapphire pavilion, joined together with a colorless cement. These are the first assemblages of synthetic spinel and synthetic sapphire observed by GIA.

*Najmeh Anjomani*

## Laminated TORTOISESHELL Scepter

"Tortoiseshell" generally refers to a material produced from the shell of the hawksbill sea turtle (T. Hainschwang and L. Leggio, "The characterization of tortoise shell and its imitations," Spring 2006 *G&G*, pp. 36–52). Because of its attractive appearance, durability, and thermoplasticity, it had been widely used for jewelry, personal items, and ornamental objects since ancient times, until the international trade of new tortoiseshell was banned in the 1970s under the Convention on International Trade in Endangered Species (www.cites.org). Today, this material is seldom submitted to gemological laboratories.

Recently, a mottled brownish orange scepter measuring 203.00 × 41.45 × 42.52 mm was submitted to GIA's Hong Kong laboratory (figure 22). The object was adorned with white metal and numerous stones of various shapes and colors.

Standard gemological testing revealed an RI of 1.56. In addition to the orange bodycolor with distinctive brown patches and resinous luster, the strong odor of burned protein given in hot point testing ruled out most inorganic and organic materials except the keratinous materials tortoiseshell and horn. Under magnification, the piece showed a layered structure and mottled color patches made up of numerous brownish dots of pigment (figure 23), both typical of tortoiseshell. The only remaining question was the thickness of the piece, which at 42.52 mm far exceeded tortoiseshell's maximum thickness of 9–12 mm (Hainschwang and Leggio, 2006). The orange part of the scepter exhibited a strong blue reaction to long-wave UV radiation, with a wavy layered struc-

*Figure 23. The brown patches in the tortoiseshell scepter were made up of numerous brownish spots. Field of view 1.88 mm.*

*Figure 24. Left: Under long-wave UV, the scepter showed disordered wavy layers of various thickness and boundary layers marked by structural discontinuities. Right: A natural tortoiseshell tablet displays a parallel layered structure in side view. Field of view 19.27 mm.*

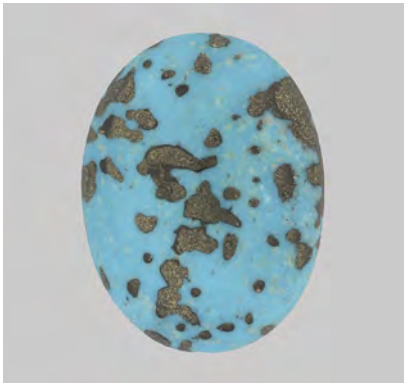

*Figure 26. A 78.60 ct greenish blue turquoise oval bead with artificial metallic pyrite. The turquoise was filled with a mixture of crushed pyrite and polymer.*

ture and distinct boundaries (figure 24, left), and a weaker reaction to short-wave UV. The brown patches were inert to both long-wave and short-wave UV. Taking into account the piece's exceptional thickness and the unusual structural discontinuities observed under UV source, we concluded this material was laminated tortoiseshell.

Further analysis by FTIR on powdered samples collected at different layers showed a keratin spectrum with predominant amide peaks at 1637, 1516, and 1236 $cm^{-1}$ (figure 25), which confirmed the material was tortoiseshell (Hainschwang and Leggio, 2006). High levels of S and Cl detected by EDXRF were also consistent with known tortoiseshell samples.

*Xiaodan Jia and Mei Mei Sit*

## TURQUOISE with Simulated Matrix

The Carlsbad laboratory recently examined a 78.60 ct greenish blue oval bead with patches that contained fragments of a metallic material in dark matrix (figure 26). Standard gemological testing of the greenish blue areas showed properties consistent with turquoise, including a refractive index of 1.60. Microscopic observations revealed the typical visual characteristics of turquoise: blue and white mottling, a granular texture, and a waxy luster with no evidence of dye. Raman analysis confirmed the metallic material was pyrite, and infrared spectroscopy indicated the greenish blue material was turquoise.

Upon closer investigation using a standard gemological microscope, it

*Figure 25. FTIR spectra of the tortoiseshell displayed amide peaks at 1637, 1516, and 1236 $cm^{-1}$. The spectrum on the right is a closer view of the region in the red box on the left.*

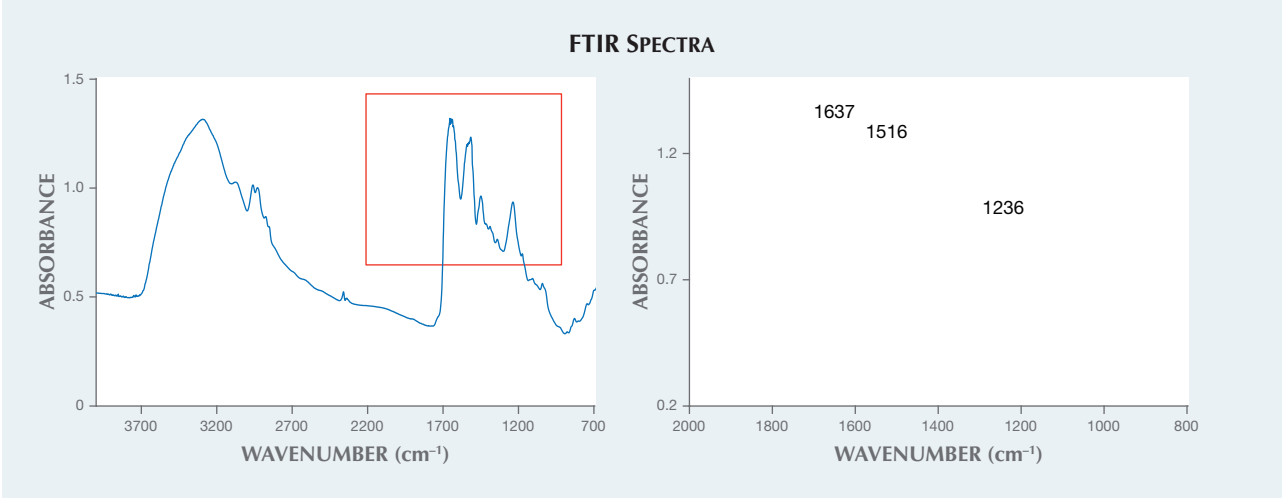

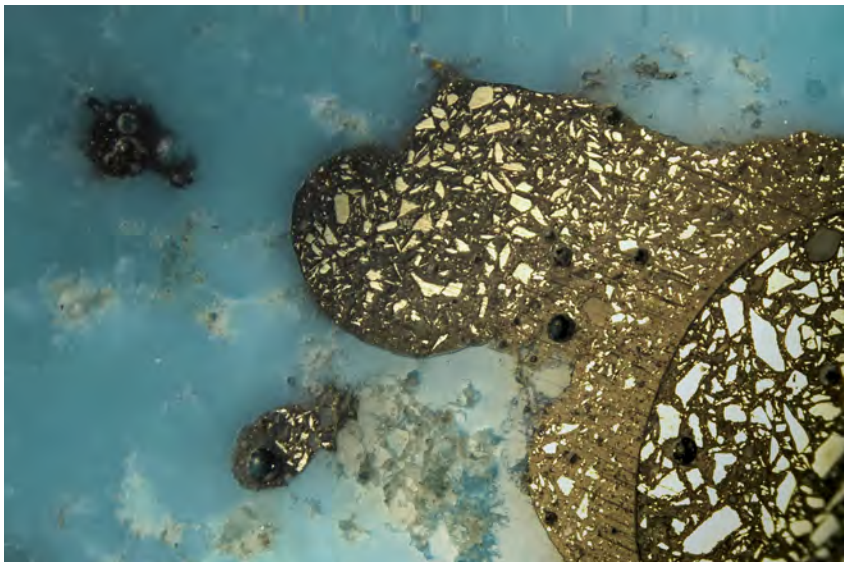

*Figure 27. Closer magnification revealed crushed pyrite crystals, voids left behind from gas bubbles, and a discontinuity between two episodes of filling. Field of view 4.02 mm.*

became clear that the pyrite was composed of irregular and angular broken fragments suspended in a fine-grained black matrix. In addition, each dark patch displayed well-defined boundaries with hemispherical voids, presumably gas bubbles that had been cut through during polishing. Interestingly, one patch showed a discontinuity between two different shades of color and textures of the pyrite in black matrix (figure 27). Based on our observations, we believe these patches were formed by filling the cavities of the turquoise with a mixture of crushed pyrite crystals and a type of polymer resin. The treatment might have involved one or more filling episodes, which could explain the discontinuity seen in one of the patches. The filled turquoise was later polished into the finished product we observed.

In the past, we have seen a variety of treatments for turquoise, but this was the first example of an artificial pyrite-containing matrix examined at the Carlsbad laboratory.

*Rebecca Tsang*

*PHOTO CREDITS:*
*HyeJin Jang-Green—1; Jian Xin (Jae) Liao—3 (left); Evan M. Smith—3 (center and right); Lhapsin Nillapat—7; Johnny Leung and Tony Leung—9, 16; Billie "Pui Lai" Law—10, 11, 12; Johnny Leung—14, 15, 24 (left); Troy Ardon—18, 19; Robison McMurtry—20; Nathan Renfro—21; Tony Leung—22; Xiaodan Jia—23; Jonathan Muyal—24 (right); C.D. Mengason—26; Rebecca Tsang and Nathan Renfro—27.*